MAGNETOHYDRODYNAMIC NON-NEWTONIAN FLOW AND HEAT TRANSFER IN A ROTATING CHANNEL

S.S.S. Mishra[1], P.K. Mishra[2], P. Paikaray[3], G.S. Ray[4], A.Mishra[5], A.P.Mishra[6]

1. **Dept. of Physics, UGS Mahavidyalaya, Sakhigopal, Puri (India)**
2. **Dept. of Physics, Bhadrak autonomous College, Bhadrak (India)**
3. **Dept. of Physics, KPAN College, Bankoi, Khurda (India)**
4. **Dept. of Physics, BJB Autonomous College, BBSR (India)**
5. **Dept. of physics, A.D. Mahavidyalaya, Brahmagiri, Puri (India)**
6. **Research Scholar.**

ABSTRACT

This paper deals with hydromagnetic non-Newtonian flow and heat transfer in a rotating channel. Constitutive equations of momentum, energy and continuity are framed. These equations are solved with the involved boundary conditions. Graphs and tables are drawn after numerical and computational analysis of the expressions of velocity and temperature of the fluid with the variation of fluid parameters. It is observed that the rotation parameter K^2 influences the flow characteristics appreciably.

Keywords : MHD, non-Newtonian flow, rotating channel, heat transfer.

1. INTRODUCTION

The MHD flow of a conducting liquid between two non-conducting parallel plates in the presence of a transverse magnetic field was studied by Hartmann[1], Agarwal[2] and Soundalgekar[3]. Shercliff[4] and Tenazawa[5] discussed the MHD flows in channels with rectangular and circular cross-section. The effects of wall conductances on hydromagnetic duct flow was studied by Chang and Lundgren[6] and that on channel flow was investigated by Chang and Yen[7]. The heat transfer aspect of the channel flow between two electrically conducting walls was presented by Yen[8]. Jagdeesen[9] and Soundalgekar[10].

The motivation of the present investigation is to extend the analysis of Chang and Yen[11] in a rotating frame of reference. The heat transfer aspect of the problem has

also been discussed. We believe that the importance of studying the simultaneous effects of the magnetic field and the coriolis forces on the problems of fluid flow lies in the fact that the study may have some bearing with the geophysical and astrophysical problems. An exact solution of the governing equations has been obtained. Nanda and Mohanty[12] have discussed the hydromagnetic flow in a rotating channel with perfectly conducting walls and his results follow as a particular case from our results. They, however, have not studied the heat transfer characteristics.

2. MHD EQUATIONS IN ROTATING FRAME

The MHD equations on motion and continuity in a rotating frame of reference for an incompressible fluid are

$$\frac{\partial \vec{q}}{\partial t} + (\vec{q}.\nabla)\vec{q} + 2\vec{\Omega}\times\vec{q} = -\frac{1}{\rho}\nabla p^{*} + \nu\nabla^{2}\vec{q} + K_0^{*}\nabla^{3}\vec{q} + \frac{1}{\rho}\vec{J}\times\vec{B},\ K_0^{*} = \frac{K_0}{\rho} \tag{1}$$

$$\nabla.\vec{q} = 0, \tag{2}$$

$$\mu_e\vec{J} = \nabla\times\vec{B}, \tag{3}$$

$$\nabla\times\vec{E} = -\frac{\partial\vec{B}}{\partial t}, \tag{4}$$

$$\nabla.\vec{B} = 0, \tag{5}$$

and the Ohm's law

$$\vec{J} = \alpha\left[\vec{E} + \vec{q}\times\vec{B}\right] \tag{6}$$

Where $\vec{q}$ is the velocity vector, $\vec{B}$ the magnetic induction. $\vec{J}$ the current density, $\vec{E}$ the electric field relative to the rotating frame. $\vec{\Omega}$ the angular velocity of the system considering the plates and the fluid referred to the fixed inertial frame and

$$p^{*} = p - \frac{1}{2}\rho\left|\vec{\Omega}\times\vec{p}\right|$$

p being the fluid pressure at a point whose distance from the axis of rotation is $\vec{p}$.

Taking curl of the equation (6) and using (3) (5), we get the magnetic induction equation as

$$\frac{\partial\vec{B}}{\partial t} = \nabla\times\left(\vec{q}\times\vec{B}\right) + \nu_m\nabla^{2}\vec{B}, \tag{7}$$

Where $\nu_m = 1/\alpha\mu_e$ is the magnetic diffusivity.

3 MATHEMATICAL FORMULATION AND ITS SOLUTION

Consider the flow within a parallel plate channel (Z=±L) due to a constant pressure gradient in the x-direction in the presence of a uniform transverse magnetic induction B_0 along z-axis about which the system is rotating with an angular velocity Ω (see Fig. 1). Considering the plates to be infinite in the x and y directions, in the steady state, the velocity and the magnetic field depend only on z. The velocity $\vec{q}$, the magnetic flux density $\vec{B}$ and the current density $\vec{J}$ may be reasonably assumed as

$$\vec{q} = (u, v, 0),\ \vec{B} = (B_x, B_y, B_0),\ \vec{J} = (j_x, j_y, 0) \tag{8}$$

Making use of (2.8) in (2.3), we get

$$\mu_e j_x = -\frac{dB_y}{dz},\ \mu_e j_y = -\frac{dB_x}{dz}, \tag{9}$$

Under the assumption (8), equations (2) and (5) are automatically satisfied. Using (8) and (9) in (1) and (7), we get

$$-2\Omega u = -\frac{1}{\rho}\frac{\partial p^*}{\partial x} + \nu\frac{d^2u}{dz^2} + K_0^*\frac{d^3u}{dz^3} + \frac{B_0}{\rho\mu_e}\frac{dB_x}{dz}, \tag{10}$$

$$2\Omega u = \nu\frac{d^2u}{dz^2} + \frac{B_0}{\rho\mu_e}\frac{dB_y}{dz} \tag{11}$$

$$0 = -\frac{1}{\rho}\frac{\partial p^*}{\partial z} - \frac{1}{\rho\mu_e}\left[K_x\frac{dB_x}{dz} + B_y\frac{dB_y}{dz}\right] \tag{12}$$

$$\frac{d^2B_x}{dz^2} + \mu_0\alpha B_0\frac{du}{dz} = 0, \tag{13}$$

$$\frac{d^2B_y}{dz^2} + \mu_0\alpha B_0\frac{du}{dz} = 0, \tag{14}$$

The absence of $\frac{\partial p^*}{\partial y}$ in equation (11) implies that there is a net cross flow along y-axis.

To derive the boundary conditions on the magnetic field at the interface between a conducting plate and the conducting fluid, we first consider the

electromagnetic filed within the plate.

Within the solid medium (say the upper plate), we have

$$j_x^{(s)} = \alpha_1 E_x\,,\ j_y^{(s)} = \alpha_1 E_y \tag{15}$$

Where a_1 is the electrical conductively of the upper plate and the superscript 's' denotes the quantities within the solid.

From the equation $\nabla \times \vec{E} = 0$, we get $E_x = E_y$ = constant within the solid boundaries as well as within the fluid. Now using (15) in the equation $\mu_e \vec{J} = \nabla \times \vec{B}$, one gets

$$\frac{dB_x^{(s)}}{dz} - \mu_e\, a_1\, E_y = 0$$

$$\frac{dB_y^{(s)}}{dz} - \mu_e\, a_1\, E_x = 0 \tag{16}$$

Since E_x and E_y are constants, the integration of (16) gives

$$\left.\begin{aligned} B_x^{(s)} &= \mu_e\, a_1\, E_y\, [-L - h_1 + z) \\ B_y^{(s)} &= \mu_e\, a_1\, E_x\, [L + h_1 - z) \end{aligned}\right\} \tag{17}$$

Where we make use of the fact that $B_x = B_y = 0$ at $z = L + h_1$. h_1 being the thickness of the upper plate.

Thus at z=L i.e. at the interface between the upper plate and the fluid, we have from (17).

$$E_y = -\frac{B_x^{(s)}}{\mu_e a_1 h_1},\ E_x = \frac{B_y^{(s)}}{\mu_e a_1 h_1} \text{ at } Z = L \tag{18}$$

Now within the liquid, we have

$$\frac{dB_x}{dz} - \mu_e a E_y = 0\,,$$

$$\frac{dB_y}{dz} - \mu_e a E_x = 0 \text{ at } Z = L \tag{19}$$

Since the tangential component of the magnetic field is continuous at the interface Z=L, using (18) in (19), we get

$$\frac{dB_x}{dz} + \frac{aB_x}{a_1 h_1} = 0$$

$$\frac{dB_y}{dz} + \frac{aB_x}{a_1 h_1} = 0 \qquad \text{at } Z = L \qquad (20)$$

Similarly, the boundary conditions of the magnetic field at the lower plate Z = –L can be derived as

$$\frac{dB_x}{dz} - \frac{aB_x}{a_2 h_2} = 0$$

$$\frac{dB_y}{dz} + \frac{aB_y}{a_2 h_2} = 0 \qquad \text{at } Z = -L \qquad (21)$$

Where a_2 and h_2 are respectively the electrical conductivity and the thickness of the lower plate.

Introducing non-dimensional variables

$$\eta = Z/L, \quad u_x = uL/\nu, \quad u_y = uL/\nu$$

$$b_x = \frac{B_x}{\sigma\mu_e B_0 \nu}, \; b_y = \frac{B_y}{\sigma\mu_e B_0 \nu} \qquad (22)$$

the equations (10), (11), (13) and (14) reduce to

$$R_c \frac{d^3 u_x}{d\eta^3} + \frac{d^2 u_x}{d\eta^2} + M^2 \frac{db_x}{d\eta} + 2K^2 u_y = -R, \qquad (23)$$

$$R_c \frac{d^3 u_y}{d\eta^3} + \frac{d^2 u_y}{d\eta^2} + M^2 \frac{db_y}{d\eta} + 2K^2 u_x = 0, \qquad (24)$$

$$\frac{d^2 b_x}{d\eta^2} + \frac{du_x}{d\eta} = 0, \qquad (25)$$

$$\frac{d^2 b_y}{d\eta^2} + \frac{du_y}{d\eta} = 0, \qquad (26)$$

Where

$$\left.\begin{aligned} R_c &= \frac{K_0^* L^2}{\nu^2}, \text{ non-Newtonian parameter} \\ M &= B_0 L \left(\frac{\sigma}{\rho\nu}\right)^{1/2} \text{ is the Hartmann number,} \\ K^2 &= \Omega \frac{L^2}{\nu} \text{ is the rotation parameter} \\ R &= \frac{L^3}{\rho\nu^2}\left(-\frac{\partial p^*}{\partial x}\right) \text{is the dimensionless pressure gradient.} \end{aligned}\right\} \quad (27)$$

The boundary conditions for the velocity components u_x and u_y are

$$u_x = u_y = 0 \text{ at } \eta = \pm 1 \quad (28)$$

The boundary conditions (20) and (21) of b_x and b_y are

$$\left.\begin{aligned} \frac{db_x}{d\eta} + \frac{b_x}{\phi_1} = 0, \ \frac{db_y}{d\eta} + \frac{b_y}{\phi_1} = 0, \ \text{at } \eta = 1, \\ \frac{db_x}{d\eta} - \frac{b_x}{\phi_2} = 0, \ \frac{db_y}{d\eta} - \frac{b_y}{\phi_2} = 0, \ \text{at } \eta = -1, \end{aligned}\right\} \quad (29)$$

Where $\phi_1 = \frac{\sigma_1 h_1}{\sigma L}$ and $\phi_2 = \frac{\sigma_2 h_2}{\sigma L}$ are the dimensionless electrical conductance rations.

Introducing the complex quantities

$$u_1 = u_x + i\, u_y,\ b = b_x + i\, b_y\ , \quad (30)$$

equations (23) – (26) give

$$\frac{d^2 u_1}{d\eta^2} + M^2 \frac{db}{d\eta} - 2\, iK^2 u_1 = -R, \quad (31)$$

$$\frac{d^2 b}{d\eta^2} + \frac{du_1}{d\eta} = 0 \quad (32)$$

Using (30), the boundary conditions (28) and (29) become

$$u_1 = 0 \quad \text{at } \eta = \pm 1, \quad (33a)$$

$$\left.\begin{aligned} \frac{db}{d\eta}+\frac{b}{\phi_1}=0 \text{ at } \eta = 1, \\ \frac{db}{d\eta}+\frac{b}{\phi_2}=0 \text{ at } \eta = -1, \end{aligned}\right\} \qquad (33b)$$

The solutions obtained for u_1 and b_1 satisfying the boundary conditions (33) are

$$u_1 = RC_1\left[1-\frac{\text{Coshmn}}{\text{Coshm}}\right]\text{Cos h m}, \qquad (34)$$

$$b = R\,[C_2\eta + \frac{C_1}{m}\text{simh m n}] + C_2^* \qquad (35)$$

where $m = \alpha + i\beta$;

$$\alpha = \frac{1}{\sqrt{2}}\left[M^2\left(M^4+4K^4\right)^{1/2}\right]^{1/2},\ \beta = \frac{1}{\sqrt{2}}\left[-M^2\left(M^4+4K^4\right)^{1/2}\right]^{1/2}$$

$$\phi = \phi_1 + \phi_2, C_1 = \frac{m(\phi+2)}{2M^2\text{simhm} + m\left(m^2\phi+4ik^2\right)\text{Coshm}}$$

$$C_2 = \frac{1}{M^2}(1-2i\,K^2C_1\,\text{Cos h m}),$$

$$C_2^* = \frac{R\left(\phi_1-\phi_2\right)}{2M^2}\,(1-C_1\,m^2\,\cos h\,m) \qquad (36)$$

The dimensionless current density j^* is given by

$$j^* = i\,R\,[C_2 + C_1\cos h\,m\,\eta], \qquad (37)$$

Where $j^* = j_x^* + ij_y^*$

It is interesting to note from the expressions of the co-efficients C_1, C_2 and C_2^* that the velocity and the current density depend only on the sum of the wall conductances ϕ_1 and ϕ_2 but the magnetic field depends on the individual values of ϕ_1 and ϕ_2.

In the absence of rotation, that is, when $K^2 = 0$,the solution (34), (35) and (37) reduce to the equations (10), (11) and (12) respectively of Chang and Yen[7].

When the plates are perfectly conducting the solution (34) and (35) reduces to

$$u_1 = \frac{R}{m^2}\left[1-\frac{\text{Coshmn}}{\text{Coshm}}\right], \tag{38}$$

$$b = -\frac{R}{m^2}\left[\eta-\frac{\text{Coshmn}}{\text{Coshm}}\right], \; m = \alpha+i\beta, \tag{39}$$

which agree with Nanda and Mohanty (1971).

4 DISCUSSION OF RESULTS

To study the effects of wall conductances and the rotation on the hydromagnetic flow in a channel, we have presented the non-dimensional velocity and current density in Figs. (2) to (5) for various values of K^2 and ϕ with $M^2 = 10.0$.

Fig. 2a shows that for small values of rotation parameter, the profiles of u_x are nearly parabolic having their vertex at the centre and that for a fixed value of K^2, the maximum of u_x decreases with increase in ϕ. As the rotation parameter K^2 increases the velocity profiles are flattered. Fig. 2b shows that for large values of K^1, the velocity u_x increases everywhere with increases in ϕ. Further, the profiles of u_x are depressed at the centre of the channel and they are symmetrical about the central line of the channel. It is also seen from the same figure that the rotation of the parallel plate channel brings in humps near the two walls indicating the occurrence of boundary layer near the walls. For very large K^2, the coriolis force and the magnetic field which act against the pressure gradient, causes reversal of the flow.

The profiles of $(-u_y)$ have been drawn against η in Figs. (3). From these figures we find that the profiles of $(-u_y)$ have similar characteristics as those of u_x when K^2 is small, but when K^2 is large the magnitude of u_y decreases with increase in ϕ.

The graphs of the current density components j_x^* and j_y^* have been plotted against η in Figs. (4) and (5). It is found from Figs. (4) that for small values of K^2, the magnitude of current density j_x^* decreases at the central region of the channel and increases near the channel walls, but for large values of K^2, the magnitude of j_x^* increases at all points with increases in ϕ. From Figs. (5) it is observed that for both high and low rotation parameter K^2, the current density j_y^* decreases throughout with increases in ϕ. Further, it can be seen that both the components of current density at

the plates decreases with increases in either K^2 or ϕ.

The non-dimensional shear-stresses components at the plate $\eta=i$ due to the primary and the secondary flow are respectively given by

$$\tau_x = \left.\frac{du_x}{d\eta}\right]_{\eta=1} \text{ and } \tau_y = \left.\frac{du_y}{d\eta}\right]_{\eta=1} \tag{40}$$

The resultant shear-stress at the plate $\eta=1$ given by

$$\tau_R = \left[\tau_x^2 + \tau_y^2\right]^{1/2} \tag{41}$$

The values of resultant shear-stress at the plate $\eta=1$ tabulated in Table 1 for various values of K^2 and ϕ with $M^2 = 10.0$. From the table 1, it is seen that the resultant shear-stress at the plate $\eta=1$ always decreases with increase in either K^1 or ϕ. For large values of K^2, the effect of ϕon the shear-stress is negligible. The resultant sheer-stress at the plate $\eta= -1$ is equal to that at $\eta=1$.

Donating Q_x^* and Q_y^* as the non-dimensional mass flow along x and y – directions respectively, we have

$$Q_x^* + i\,Q_y^* = \frac{i}{2}\int_{-1}^{1} u_1 d\eta$$

$$= RC_1\left[\frac{Sinhm}{m} - Coshm\right] \tag{42}$$

The values of $\frac{Q_x^*}{R}$ and are given in Table 2 and 3 for various values of K^2 and ϕ with $M^x = 1.0$. From the table 2. It is seen that with increase in ϕ, $\frac{Q_x^*}{R}$ decreases when K^2 is small and it increases when K^2 is large. For fixed value of ϕ, $\frac{Q_x^*}{R}$ decreases with increase in K^2 and for large K^2 the mass flow $\frac{Q_x^*}{R}$ is negligible. Table 3 shows that $\left(-\frac{Q_x^*}{R}\right)$ decreases with increase in either K^2 or ϕ.

For perfectly conducting walls the mass flow given by (42) should agree to

equation (31) of Nanda and Mohanty[10]. Unfortunately, a little calculation shows that the expression for the mass-flow given in equation (31) of Nanda and Mohanty[10] is wrong. This renders the results presented in Tables II and III in their paper to be erroneous. The correct form of the equation (31) of Nanda and Mohanty[10] is

$$\frac{Q_x + iQ_y}{\rho\nu} = \frac{R(\alpha-\beta)}{(\alpha^2+\beta^2)^3}\left[(\alpha+i\beta) - \tanh(\alpha+i\beta)\right] \tag{43}$$

Where α and β are given by equation (36). The correct results for Q_x and Q_y have been presented in Table (4a, b) for various values of M^2 and K^2.

5. HEAT TRANSFER

The equation of energy for steady fully developed state is given by

$$0 = \alpha_1 \frac{d^2T}{dz^2} + \frac{\mu}{\rho C_p}\left[\left(\frac{du}{dz}\right)^2 + \left(\frac{du}{dz}\right)^2\right] + \frac{1}{\sigma\mu_e^2\rho\varepsilon_p}\left[\left(\frac{dB_x}{dz}\right)^2 + \left(\frac{dB_x}{dz}\right)^2\right] \tag{44}$$

Where T is the temperature taken as a function of Z only, α_1 is the thermal diffusivity and C_p is the specific heat of the fluid. The last two terms within the parentheses represent the viscous and Ohmic dissipations respectively. Introducing

$$\theta(\eta) = \frac{T-T_1}{T_2-T_1}, P_r = \nu/\alpha_1, \frac{\nu^2}{C_p(T_1-T_1)L^2} \tag{45}$$

and using (22) in (44), we get

$$\frac{d^2\theta}{d\eta^2} + P_r E_c\left[\left(\frac{du_x}{d\eta}\right)^2 + \left(\frac{du_y}{d\eta^2}\right)^2 + M^2\left\{\left(\frac{db_x}{d\eta}\right)^2 + \left(\frac{db_y}{d\eta}\right)^2\right\}\right] = 0 \tag{46}$$

Where T_1 and T_2 denote the temperature of the lower and upper plates respectively, P_r is the Prandtl number and E_c is the non-dimensional parameter.

The boundary conditions for $\theta(\pm)$ are

$$\theta(-1) = 0, \theta(1) = 1 \tag{47}$$

On introducing the complex quantities, given by (30), the equation (46) reduces to

$$\frac{d^2\theta}{d\eta^2} + P_r E_c \left[\frac{du_1}{d\eta}, \frac{du_1}{d\eta} + M^2 \frac{db}{d\eta} \frac{db}{d\eta} \right] = 0 \qquad (48)$$

Where the over bar denotes complex conjugate.

Using (34) and (35), the selection of (48) satisfying the boundary conditions (47) is given by

$$\theta(\eta) = -\frac{P_r}{M^2} E_c R^2 \left[a_0 M^2 \left(a_1 \text{Cosh}\alpha\eta \text{Cos}\beta\eta - a_2 \text{Sinh}\alpha\eta \text{Sin}\beta\eta \right) + \right.$$

$$+2\, a_0 K^2 (a_2 \text{ Cos h } \alpha\eta \text{ Cos } \beta\eta + a_1 \text{ Sin h } \alpha\, \eta \text{ Sin } \beta\, \eta) +$$

$$+ \frac{a_3}{4K^4} (\beta^2 \text{ Cos h } 2\alpha\, \eta - \alpha^2 \text{ Cos } 2\beta\eta) - \frac{1}{2} (1 + a_4 + a_5)\eta^2]$$

$$- \frac{a_6}{4K^4} (\beta^2 \text{ Cos h } 2\alpha\, \eta + \alpha^2 \text{ Cos } 2\beta\eta) + \frac{1}{2}\, \eta + a_7 \qquad (49)$$

Where

$a_0 = \dfrac{2}{M^4 + 4K^4}$, $a_1 = -M^2 (A_7 + 2K^2\, a_8 \text{ sin h } \alpha \text{ Sin } \beta)$

$a_2 = -M^2 (A_8 + 2K^2\, a_8 \text{ Cos h } \alpha \text{ Cos } \beta)$, $a_3 = \dfrac{1}{2} M^4\, a_8$,

$a_4 = 4K^2 (A_8 \text{ Cos h } \alpha \text{ Cos } \beta + A_7 \text{ Sin h } \alpha \text{ Sin } \beta)$,

$a_5 = 2\, K^4 a_8 (\text{Cos h } 2\, \alpha + \text{Cos } 2\beta)$, $a_6 = \dfrac{P_7}{2} E_c\, R^2\, a_8\, (\alpha^2 + \beta^2)$

$a_7 = \dfrac{1}{2} + \dfrac{1}{2} (\beta^2 \text{ Cos h } 2\alpha + \alpha^2 \text{ Cos } 2\beta) + \dfrac{P_7}{2} E_c\, R^2$

$[a_0\, M^2 (a_1 \text{ Cos h } \alpha \text{ Cos } \beta - a_2 \text{ Sin h } \alpha \text{ Sin } \beta) +$

$+2\, a_0\, K^2 (a_2 \text{ Cos h } \alpha \text{ Cos } \beta + a_1 \text{ Sin h } \alpha \text{ Sin } \beta) + \dfrac{1}{2} (1 + a_2 - a_3)$

$+ \dfrac{1}{2} (\beta^2 \text{ Cos h } 2\alpha - \alpha^2 \text{ Cos } 2\beta)]$,

$a_8 = A_7^2 + A_8^2$, $A_1 = \dfrac{(1 + \text{Cot}^2\beta)\text{Coth}\alpha}{\text{Cot}^2\beta + \text{Coth}^2\alpha}$

$$A_2 = \frac{\text{Cosh}^2\alpha\text{Cos}\beta}{\text{Cot}^2\beta + \text{Coth}^2\alpha} \quad A_3 = \text{Sin h } \alpha \text{ Cos } \beta$$

$$A_4 = \text{Cos h } \alpha \text{ Sin } \beta$$

$$A_5 = M^2 (2 + \phi, \alpha A_1 + \beta A_2) - 2K^2 (\phi+) (\beta A_1 - \alpha A_2)$$

$$A_6 = 2K^2 \{2+\phi (\alpha A_1+\beta A_1\} + M^2 \phi$$

$$(\beta A_1 - \alpha A_2 - 4K^2 (1-\alpha A_1 - \beta A_1),$$

$$A_7 + i A_8 = \frac{(\phi + 2)(\alpha + i\beta)}{(A_3A_5 - A_4A_6) + i(A_4A_5 + A_3A_6)} \qquad (50)$$

From the expression (49) and (50), it is seen that the temperature also depends on the sum of the ratio of the wall conductance ϕ_1 and ϕ_2.

To study the effects of wall conductance, rotation and Hartmann number, we have computed the rate of heat transfer at the plate $\eta = 1$ for $P_r = .025$, R=1, E_c=2.0 and they are presented in Tables 5 and 6. From these tables, it is seen that with increase in either ϕ or M, the rate of heat transfer increases when K^2 is small and decreases when K^2 is large. It is also seen that for fixed M and ϕ, it increases with increase in K^2.

Finally, we can conclude that the effect of electrical conductance ratio on the velocity field, current density, shear-stress and the rate of heat transfer is similar to that of the magnetic field.

Table 1

Values of τ_R for M^2 = 10.0

ϕ/K^2	**1.0**	**4.0**	**25.0**	**81.0**
0.0	.889157	.470461	.145360	.078904
0.5	.657298	.426852	.144628	.078842
1.0	.557050	.397645	.144042	.078796
1.5	.501681	.3778592	.143576	.078760
2.0	.466660	.363178	.143203	.078731
∞	.312171	.279828	.140045	.078793

Table 2

Values of Q_x^*/R for $M^2 = 10.0$

ϕ/K^2	**1.0**	**4.0**	**25.0**	**81.0**
0.0	.173400	.046986	.002234	.000353
0.5	.135253	.054214	.002870	.000421
1.0	.116532	.056036	.003282	.000466
1.5	.105751	.056316	.003570	.000498
2.0	.098792	.056115	.003782	.000522
∞	.067044	.050005	.005161	.000688

Table 3

Values of $\left(-Q_y^*/R\right)$ for $M^2 = 10.0$

ϕ/K^2	**1.0**	**4.0**	**25.0**	**81.0**
0.0	.083867	.085222	.018104	.005838
0.5	.044513	.069692	.017921	.005829
1.0	.031339	.060213	.017775	.005822
1.5	.025053	0.54121	.017659	.005817
2.0	.021440	.049949	.017568	.005812
∞	.008851	.029155	.016800	.005777

Table 4a

Values of $\left(\frac{Q_x}{RP\nu}\right)$ for perfectly conducting walls

M^2/K^2	**1.0**	**4.0**	**25.0**	**81.0**
0.5	.192529	.037317	.002169	.000360
1.0	.180017	.041186	.002338	.000377
3.0	.135045	.051175	.003003	.000447
9.0	.072158	.050933	.004855	.000654
12.0	.058264	.046062	.005674	.000756

Table 4b

Values of $\left(-\frac{Q_y}{RP\nu}\right)$ for perfectly conducting walls

M^2/K^2	**1.0**	**4.0**	**25.0**	**81.0**
0.5	.126963	.090387	.017968	.005828
1.0	.101528	.086570	.017933	.005826
3.0	.048131	.070166	.017762	.005818
9.0	.012163	.033924	.016973	.005784
12.0	.007767	.024369	.016447	.005762

Table 5

Values of $\left.\frac{d\theta}{d\eta}\right]_{\eta=1}$ for $M^2 = 10.0$

ϕ/K^2	**1.0**	**4.0**	**25.0**	**81.0**
0.0	.487594	.497045	.499885	.499982
0.5	.491877	.497109	.499875	.499981
1.0	.493200	.497076	.499862	.499980
1.5	.493796	.497030	.499849	.499978
2.0	.494125	.496988	.499838	.499977
∞	.495130	.496637	.499719	.499964

Table 6

Values of $\left.\frac{d\theta}{d\eta}\right]_{\eta=1}$ for $\phi = 0$

M^2/K^2	**1.0**	**4.0**	**25.0**	**81.0**
0.5	.484868	.497480	.499892	.499982
10.0	.487594	.497045	.499885	.499982
20.0	.490301	.496743	.499870	.499981

Table 6 : Values of $\left.\frac{d\theta}{d\eta}\right]_{\eta=1}$ for $\phi = 0$

M^2/K^2	**1.0**	**4.0**	**25.0**	**81.0**
0.5	.490828	.496407	.499808	.499973
10.0	.495130	.496637	.499719	.499964
20.0	.497520	.497795	.499585	.499946

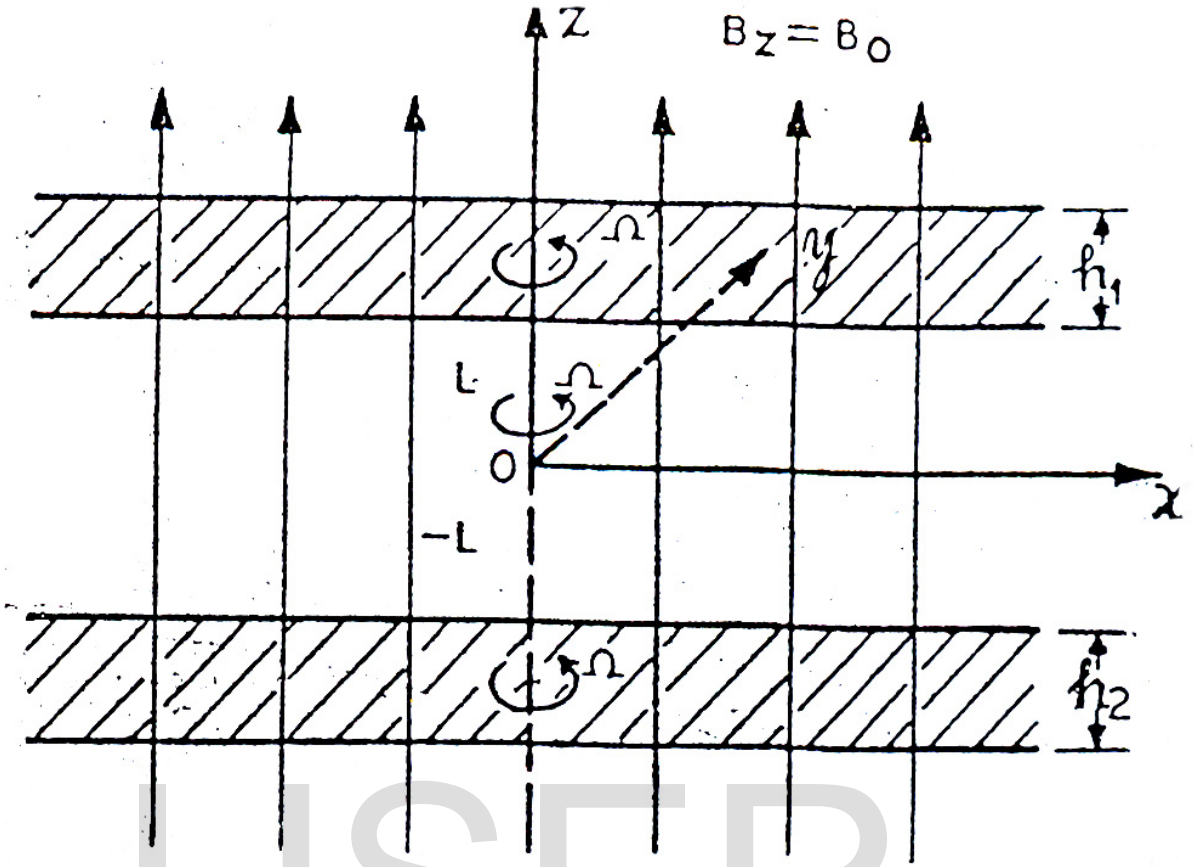

Fig. 1 : Physical Model

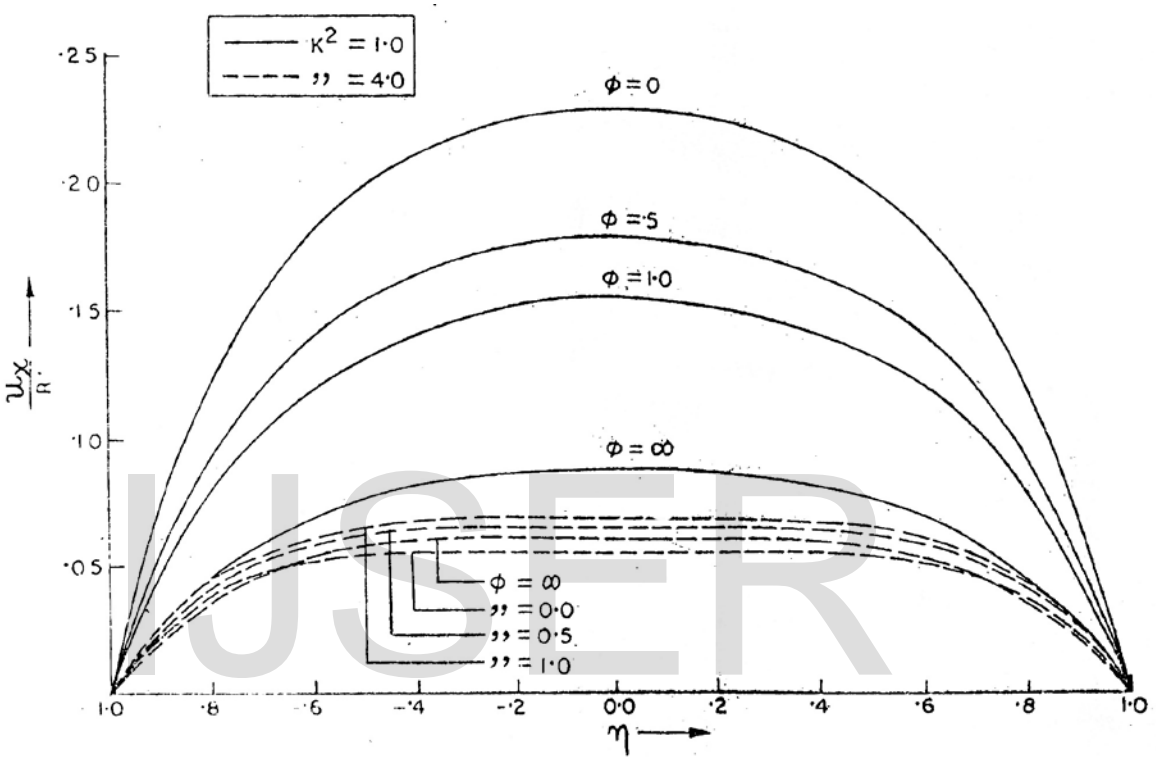

Fig. 2a : Profiles of velocity in x-direction for low K^2.

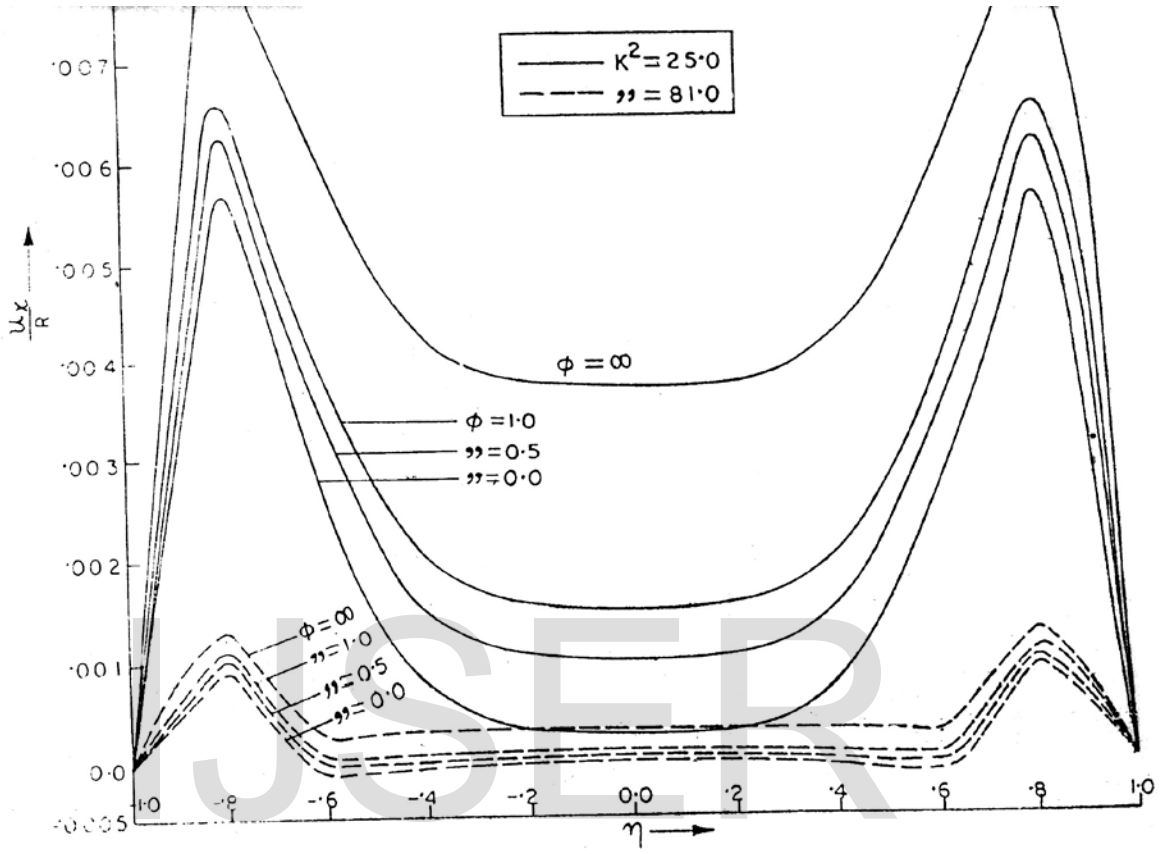

Fig. 2b : Profiles of velocity in x-direction for low K^2.

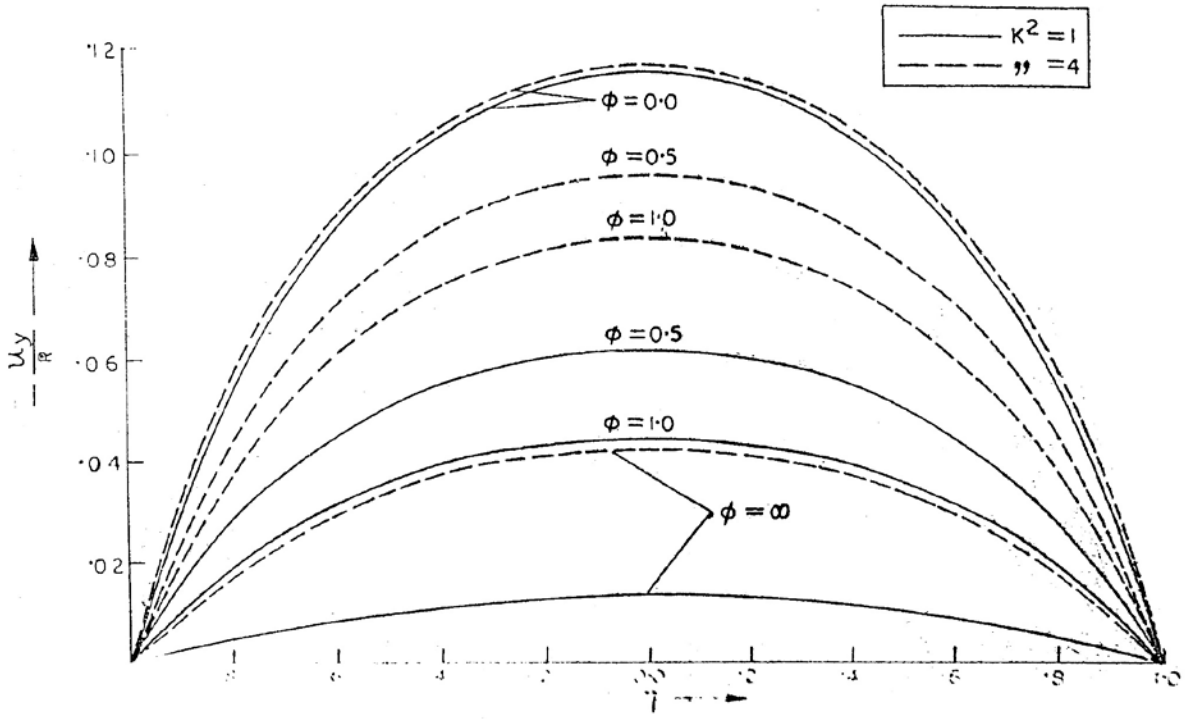

Fig. 3a : Velocity profiles in y-direction for low K^2.

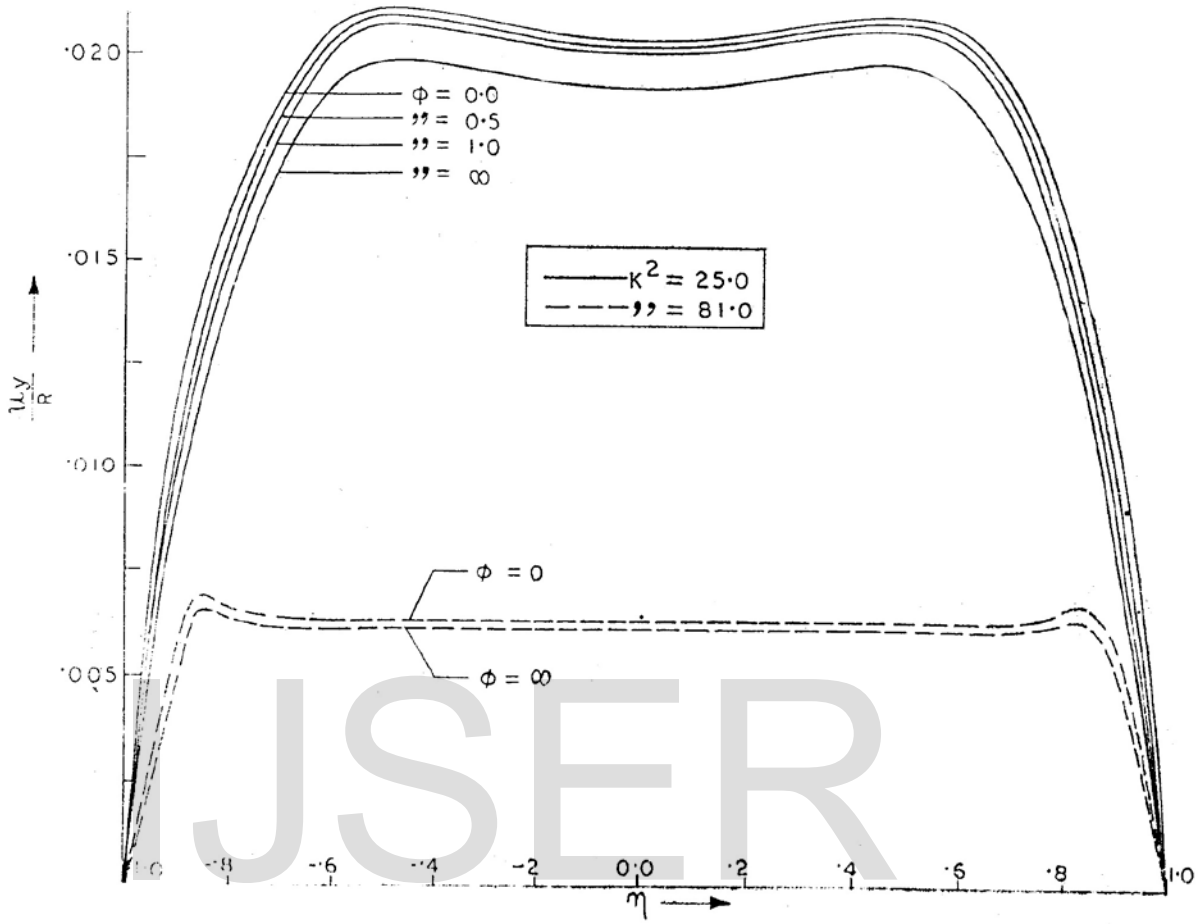

Fig. 3b : Profiles of velocity in y-direction for low K^2.

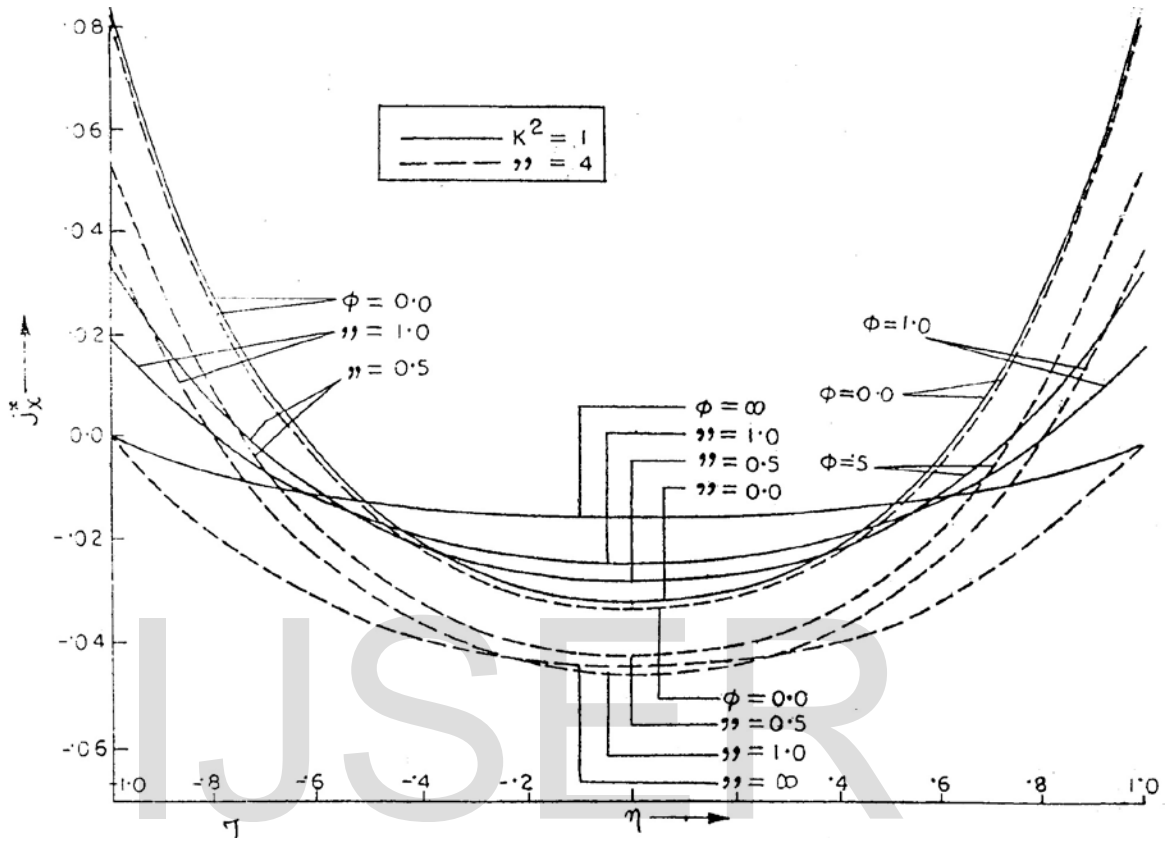

Fig. 4a : Profiles of current density j_x^* for low K^2.

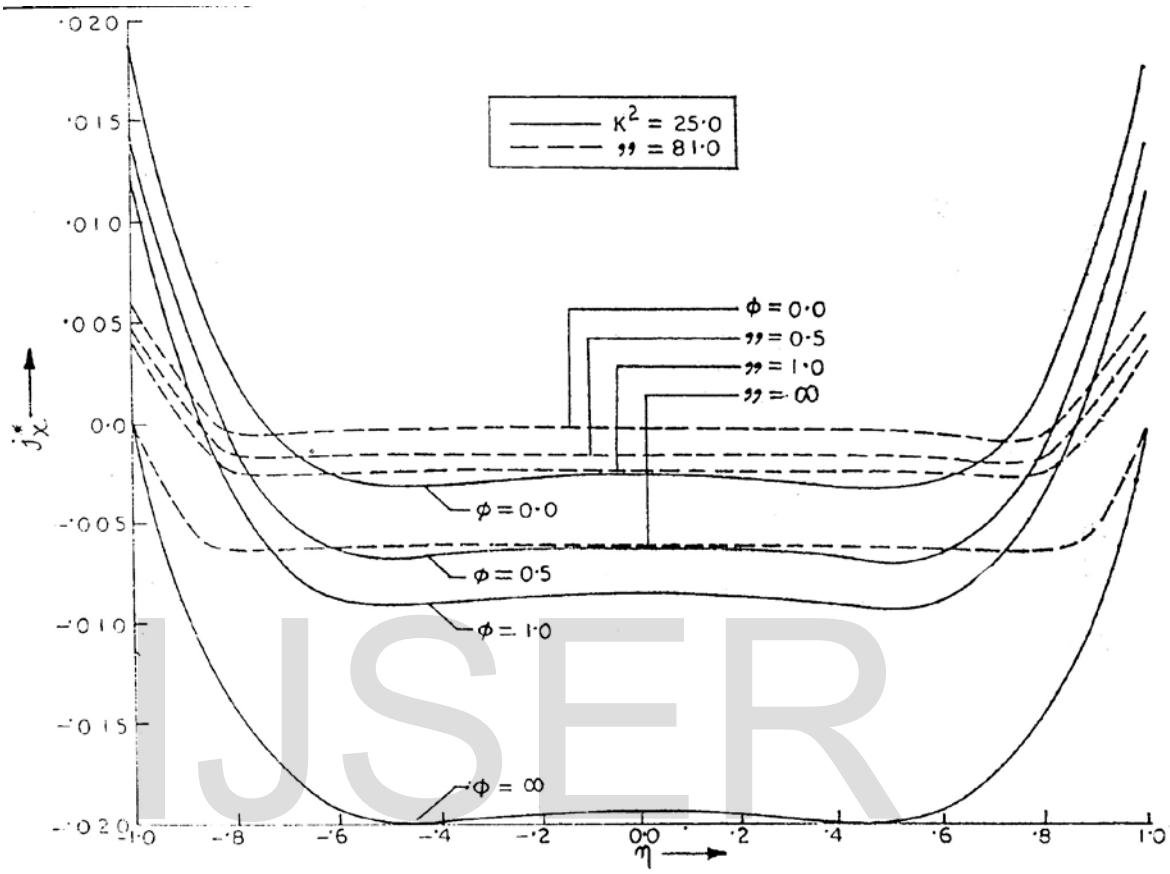

Fig.4b : Profiles of current density j_x^* for high K^2.

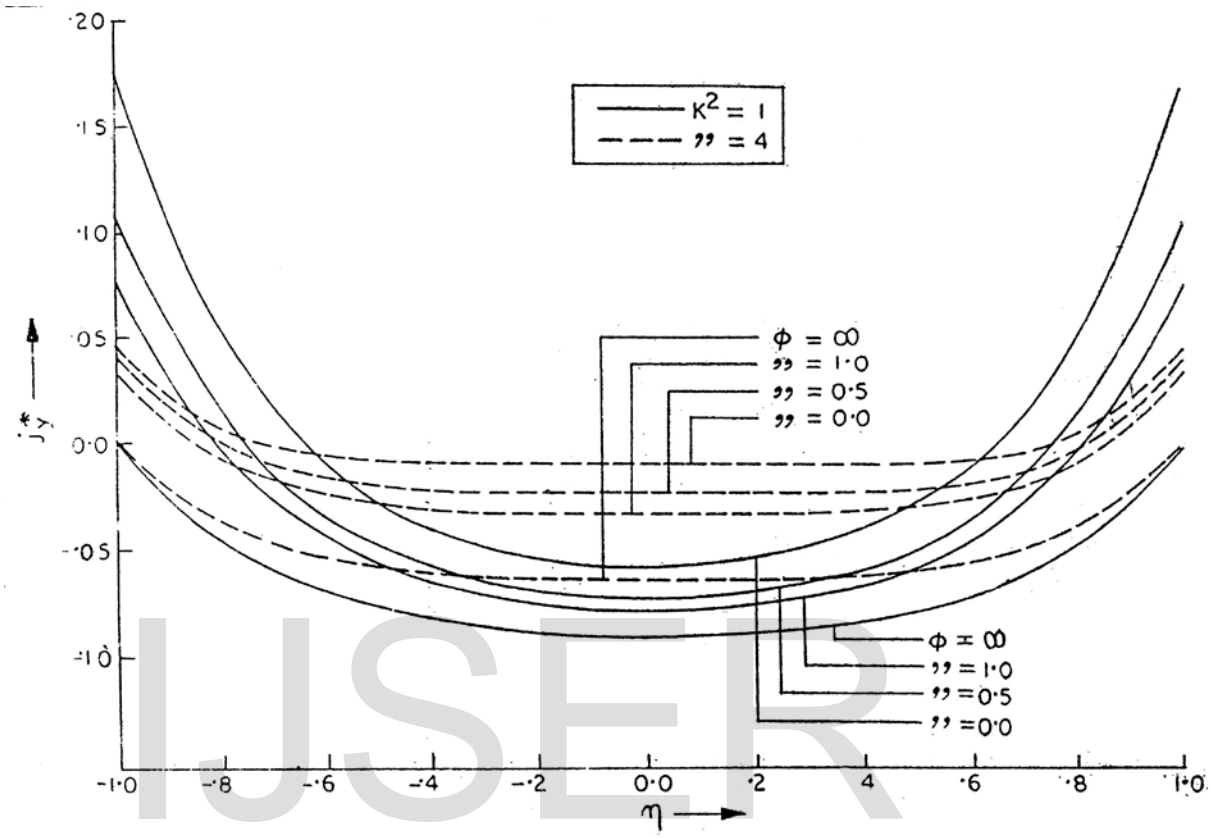

Fig. 5a : Profiles of current density j_y^* for low K^2.

REFERENCES

1. Hartmann, J. and Lazarus, F., Kgl. Danskevidensk. Selskab, *Mat. Fys*., Medd 15, 36 and 7 (1937)
2. Agarwal, J.P., *Appl. Sci. Res*., 9B, 254 (1962)
3. Soundalgekar, V.M., *Appl. Sci. Res*., 12B, 151 (1965)
4. Sheretiff, J.A., *ZAMP*, 28, 449 (1977)
5. Tenazawa, I., *Theo. Appl. Mech*., Japan (1960)
6. Lundgren, T.S. et. al, *Phys. Fluids*, 4, 100b (1961)
7. Chang, C.C. and yen, J.T., *phys. Fluids*, 2, 393 (1959)
8. Yen, J.T., *J. Heat Transfer*, Tr. ASME, 85C, 371 (1963)
9. Jagdeesen, K., *AIAA* J., 2, 75b (1964)
10. Soundalgekar, V.M., *Proc., Nat. Inst. Sci*., 35, 329 (1969)
11. Yang, K.T. *J. Appl. Mech*., 27, 230 (1962)
12. Nanda, R.S. and Mahanty, H.K., *J. Phys. Soc., Japan*, 29, 1608 (1970)
13. Chang, C.C. and Yen. J.T., *ZAMP*, 13, 266 (1962)